Moments and Distribution Functions for Polypeptide Chains. Poly-L-alanine

Joan C. Conrad and Paul J. Flory*

Department of Chemistry, Stanford University, Stanford, California 94305.
Received August 25, 1975

ABSTRACT: Statistical mechanical averages of vectors and tensors characterizing the configurations of polypeptides have been calculated for poly-L-alanines (PLA) of x_u = 2–400 peptide units. These quantities are expressed in the reference frame of the first peptide unit, the X axis being situated along the virtual bond, the Y axis in the plane of the peptide unit. The persistence vector $\mathbf{a} \equiv \langle \mathbf{r} \rangle$ converges rapidly with chain length to its limit $\mathbf{a}_\infty$ which lies virtually in the XZ plane. Configurational averages of Cartesian tensors up to the sixth rank formed from the displacement vector $\boldsymbol{\rho} = \mathbf{r} - \mathbf{a}$ have been computed. For $x_u > 50$ the even moments of fourth and sixth rank formed from the reduced vector $\tilde{\boldsymbol{\rho}}$ for the real chain are well repreented by the freely jointed chain with 21.7 virtual bonds equivalent to one of the model. The moments of $\tilde{\boldsymbol{\rho}}$ display asymmetry for $x_u < 50$. Density distribution functions $W_a(\boldsymbol{\rho})$, evaluated from the three-dimensional Hermite series truncated at the term in the polynomial involving the tensors of $\boldsymbol{\rho}$ of sixth rank, display no obvious symmetry for $x_u < 50$. Approximate spherical symmetry of the distribution of $\boldsymbol{\rho}$ about $\mathbf{a}$ is observed only for $x_u \geq 100$.

The chiral centers in polypeptides $(\text{CHR–CO–NH–})_{x_u}$ destroy the symmetry that otherwise would obtain with respect to the planes defined by successive pairs of skeletal bonds. The persistence vector $\mathbf{a} \equiv \langle \mathbf{r} \rangle$ averaged within a reference frame defined by the skeletal bonds of the initial peptide unit consequently may be expected in general to include a finite z component perpendicular to the plane of these bonds, i.e., to the plane of the initial peptide unit. For the same reason, none of the elements of the Cartesian tensors formed from the displacement vector $\boldsymbol{\rho} = \mathbf{r} - \mathbf{a}$ reduce identically to zero when averaged over all configurations of a chain of finite length.

The polypeptide chain differs importantly in another respect from the PDMS chains treated in the preceding paper[1] and from the polymethylenes CH_3–$(CH_2)_n$–H (PM) previously investigated[2] from the same standpoint. Whereas the bond rotations in PDMS and PM are consecutively neighbor dependent throughout the chain, the values assumed by the torsional angles φ_i and ψ_i (see Figure 1) specifying rotations about the bonds flanking a given C_i^α at the junction between two peptide units are independent of the rotations at neighboring alpha carbons, e.g., of the corresponding pair φ_{i-1}, ψ_{i-1} at C_{i-1}^α.[3] Hence, conformational correlations are not perpetuated from one φ,ψ pair to the next. Each such pair may be treated independently of the others, and averaging may therefore be performed over individual pairs φ,ψ with consequent simplification of the mathematical methods.

For the reasons cited above together with the significance of polypeptides as biopolymers, the investigation of the characteristics of the spatial configuration of the polypeptide chain assumes special importance.

The character of the polypeptide chain must obviously depend on the chiral senses of its asymmetric C^α centers. Polypeptides of uniform chirality, e.g., the L-polypeptides, command foremost attention. Here we shall be concerned with the prototype of this class, namely, poly-L-alanine (PLA). Comparatively high extensions are favored in polypeptide chains, exemplified by PLA, owing to the preference for conformations in the β domain of the familiar Ramachandran diagram[4] delineating conformations in φ,ψ that are free of steric overlaps, or of the corresponding conformational energy map[3,5] in which contours of calculated energies are plotted over the domain of these rotational angles φ and ψ about the N–C^α and C^α–C' bonds, respectively.

Persistence vectors for polyglycine and for PLA have been calculated by Premilat and Hermans[6] using both analytical and Monte Carlo methods. They have been evaluated approximately for PLA by Hesselink[7] using the latter methods. Both investigations show the average component $\langle z_\infty \rangle$ normal to the plane of the initial peptide unit to be fairly large; it exceeds half the magnitude of the in-plane projection of $\mathbf{a}_\infty$.

Premilat and Hermans,[6] stressing the importance of the statistics of short polypeptide chains, estimated the radial distribution $w(r)$ of the magnitude r of the chain vector $\mathbf{r}$ for PLA chains of 5, 10, 15, and 20 units using Monte Carlo methods. They further attempted to assess the spatial density distribution $W(\mathbf{r})$ for x_u = 10 units from planar projections of the numbers of Monte Carlo chains ending in layers of 3 Å depth normal to an arbitrary axis. Densities along the direction of the persistence vector suggested approximate cylindrical symmetry about this axis for these short chains.

Hesselink[7] investigated both the radial distribution $w(r)$ of the chain vector and the radial distribution $w_a(\rho)$ of the persistence vector, again on the basis of chains generated by Monte Carlo methods. The distribution of ρ was more nearly Gaussian than the distribution of r for chains of 40 and of 80 units.

In this paper we evaluate the persistence vector $\boldsymbol{\rho}$ and the configuration-averaged Cartesian tensors formed from $\boldsymbol{\rho}$ up to sixth rank as functions of chain length. The computations were carried out using matrix multiplication methods based on exact analytical relationships.[8,9] From the moment tensors, we have attempted to characterize the spatial density distributions for PLA chains of finite length.

Structural Geometry and Averaged Transformation Matrices

A portion of an all-trans poly-L-alanine chain is depicted in Figure 1. Bond angles and bond lengths are assigned the values used previously.[3,5] The angles η and ξ formed by the virtual bond vector and the N–C^α and C^α–C' skeletal bonds (see Figure 1) are 22.2 and 13.2°, respectively. The length of the virtual bond vector l_u of the trans peptide unit is 3.80Å.

A coordinate system is affixed to each peptide unit as indicated in Figure 1. The X axis of unit $i + 1$ is taken along its virtual bond; the Y axis is situated in the plane of the peptide unit with its direction making an acute angle with the amide C'–N bond of the same peptide unit; and the Z axis is assigned the direction normal to the plane of the unit required for a right-handed coordinate system.

Transformation $\mathbf{T}_i$ from the reference frame of virtual

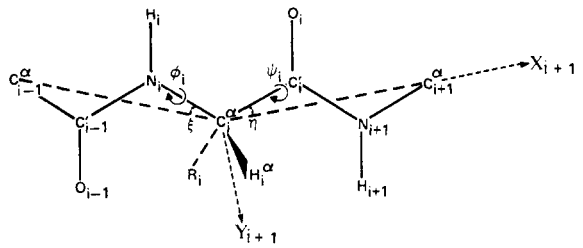

Figure 1. A portion of the all-trans poly-L-alanine chain in its planar, fully extended conformation ($\varphi = \psi = 0$). Virtual bonds connecting successive α carbons are shown by light dashed lines. The reference frame affixed to the ith peptide unit is indicated.

bond $i + 1$ to that of virtual bond i is achieved by th successive application of three rotational matrices **R**, according to the following prescription:

$$\mathbf{T}_i = \mathbf{T}(\varphi_i,\psi_i) = \mathbf{R}(\xi,0)\mathbf{R}(\theta^\alpha,\pi - \varphi_i)\mathbf{R}(-\eta,-\psi_i) \quad (1)$$

where Θ^α is the supplement of the skeletal bond angle at C^α, and

$$\mathbf{R}(\alpha,\beta) = \begin{bmatrix} \cos\alpha & \sin\alpha & 0 \\ -\sin\alpha\cos\beta & \cos\alpha\cos\beta & \sin\beta \\ \sin\alpha\sin\beta & -\cos\alpha\sin\beta & \cos\beta \end{bmatrix} \quad (2)$$

Conformational energy calculations were performed at 30° intervals of φ and ψ according to methods described previously.[3,5] The parameters used by Brant, Miller, and Flory[5] to characterize the nonbonded interactions were employed in the present calculations. Their assignments of partial charges and the effective dielectric constant were likewise adopted to express the Coulombic interactions.

The averaged transformation matrix for the ith peptide unit was calculated according to

$$\langle \mathbf{T}_i \rangle = z^{-1} \sum_{\varphi_i} \sum_{\psi_i} \mathbf{T}(\varphi_i,\psi_i) \exp[-E(\varphi_i,\psi_i)/RT] \quad (3)$$

where z is the configuration partition function for a repeat unit given by

$$z = \sum_{\varphi_i} \sum_{\psi_i} \exp[-E(\varphi_i,\psi_i)/RT] \quad (4)$$

All calculations were performed for a temperature of 25°C.

The summations were performed over values of the argument at intervals of 30° in φ_i and ψ_i. Conformations for which $E(\varphi_i,\psi_i)$ exceeds its minimum value by more than 4.0 kcal mol^{-1} were omitted from the sums inasmuch as their contributions are quite negligible. Averaged transformation matrices of higher orders ($\langle \mathbf{T}_i^{\times p} \rangle$; see below) were evaluated in like manner.

The averaged transformation matrix computed for the PLA chain as described above is:

$$\langle \mathbf{T} \rangle = \begin{bmatrix} 0.50 & 0.18 & 0.61 \\ -0.035 & -0.62 & 0.19 \\ 0.66 & -0.21 & -0.32 \end{bmatrix} \quad (5)$$

This matrix differs trivially from the one evaluated by Brant, Miller, and Flory.[5] Small differences in the elements, which do not exceed ±0.02, are presumed to arise from our neglect of conformations for which the energy exceeds the lowest value by more than 4.0 kcal mol^{-1}.

The Persistence Vector

Since the peptide units of the PLA chain are identical and independent as well, the average of the serial product $\mathbf{T}_1^{(x_u)}$ of these transformations, $\mathbf{T}_1 \ldots \mathbf{T}_{x_u}$ inclusive, is just the product of their averages, i.e., $\langle \mathbf{T}_1^{(x_u)} \rangle = \langle \mathbf{T} \rangle^{x_u}$. Hence, if the virtual bond of each peptide unit is expressed in its own reference frame, the persistence vector[1,8,9] is given by

$$\mathbf{a} \equiv \langle \mathbf{r} \rangle = \sum_{1}^{x_u} \langle \mathbf{T} \rangle^{i-1} \boldsymbol{l}_u \quad (6)$$

where $\boldsymbol{l}_u$ is the column vector that represents the virtual bondin the reference frame of the unit, its elements being l_u, 0, 0. Alternatively, **a** is given by[8,9]

$$\mathbf{a} = \langle \mathbf{A}_{[1} \rangle \langle \mathbf{A} \rangle^{x_u-2} \mathbf{A}_{x_u]} \quad (7)$$

where **A** denotes the generator matrix defined by

$$\mathbf{A} = \begin{bmatrix} \mathbf{T} & \boldsymbol{l}_u \\ \mathbf{0} & 1 \end{bmatrix} \quad (8)$$

for an internal unit, **0** being the null matrix of 1 × 3 order. The terminal generators are

$$\mathbf{A}_{[1} = [\mathbf{T} \quad \boldsymbol{l}_u] \quad (9)$$

and

$$\mathbf{A}_{x_u]} = \begin{bmatrix} \boldsymbol{l}_u \\ 1 \end{bmatrix} \quad (10)$$

Angle brackets in eq 7 denote the configurational averages obtained by replacing **T** with $\langle \mathbf{T} \rangle$.

Persistence vectors were calculated using these relationships for chains of lengths x_u = 2 to 800 units, with $\langle \mathbf{T} \rangle$ averaged at 25°C (see above). The components converge to limiting values of $\langle x_\infty \rangle$ = 20.18 Å, $\langle y_\infty \rangle$ = 0.70 Å, and $\langle z_\infty \rangle$ = 9.98 Å. These values are approached within 0.5% at x_u = 32. Ratios $\langle x \rangle/\langle x_\infty \rangle$, etc., are plotted in Figure 2. The curve for $\langle z \rangle/\langle z_\infty \rangle$ very nearly coincides with that for $\langle x \rangle/\langle x_\infty \rangle$ and hence is not shown. The ratio $\langle y \rangle/\langle y_\infty \rangle$ displays even–odd alternation for $x_u < 15$. Inasmuch as values of $\langle y \rangle$ are small for all chain lengths x_u, this erratic behavior is of little significance. In the limit $x_u \to \infty$ the persistence vector forms angles of 26.4, 91.8, and 63.7° with the X, Y, and Z axes, respectively, of the initial unit; i.e., it is very nearly parallel to the XZ plane.

Expressed as ratios to the length l_u = 3.80 Å of the virtual bond, the limiting components of **a** are: $\langle x_\infty \rangle/l_u$ = 5.31, $\langle y_\infty \rangle/l_u$ = 0.18, and $\langle z_\infty \rangle/l_u$ = 2.63. The calculations of Premilat and Hermans[6] yield values for these ratios as follows: 4.40, −0.03, 2.58, respectively, after conversion to the same reference frame we have used.[15] Departures of our results from theirs may be presumed to arise from differences

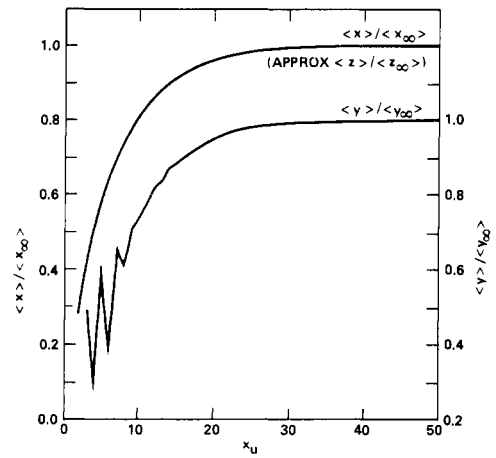

Figure 2. The components of the persistence vector **a** at 25°C as a function of the number of peptide units. Each component is divided by its value at $x_u = \infty$.

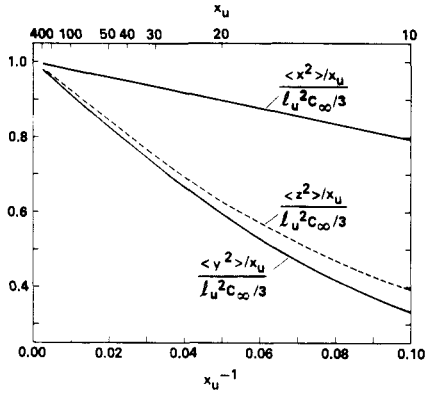

Figure 3. The diagonal components of the second moment tensor $\langle \mathbf{r}^{\times 2}\rangle$ averaged at 25°C and plotted against the reciprocal of the number of peptide units. Each component is divided by the limiting value $l_u^2C_\infty/3$.

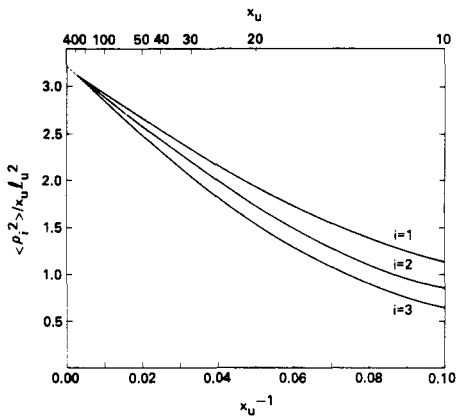

Figure 4. Principal components of the second moment tensor $\langle \rho\rho^T\rangle$ formed from the displacement vector $\rho = \mathbf{r} - \mathbf{a}$ plotted against $1/x_u$. Each component is divided by $x_u l_u^2$.

between the averaged transformation matrices $\langle \mathbf{T}\rangle$ used in the respective calculations. Their transformation matrix was averaged over a conformational energy surface differing appreciably from ours. By substitution of $\langle x_\infty\rangle = 20.18$ Å for the Porod–Kratky *persistence length* a_{PK} into eq 9 of the preceding paper, we obtain

$$C_\infty = \lim_{x_u\to\infty} (\langle r^2\rangle_0/x_u l_u^2) = 9.62$$

for the characteristic ratio at 25°C. The computations of Premilat and Hermans give $C_\infty = 7.80$. Experimental results for polypeptides analogous to PLA are in the range 8.2 to 9.6.[10–12]

Second Moments

The quadratic moments of the Cartesian tensor $\langle \mathbf{rr}^T\rangle$ formed from the chain vector $\mathbf{r}$, and comprising the elements $\langle x^2\rangle$, $\langle xy\rangle$, etc., are given in the form of a column vector by

$$\langle \mathbf{r}^{\times 2}\rangle = \langle \mathbf{A}_{[1}{}^{\times 2}\rangle \langle \mathbf{A}^{\times 2}\rangle^{x_u-2}\mathbf{A}_{x_u]}{}^{\times 2} \qquad (11)$$

where the superscript ×2 denotes the direct product of second order, i.e., $\mathbf{A}^{\times 2} = \mathbf{A} \otimes \mathbf{A}$. These generator matrices were condensed from 16 × 16 to 10 × 10 order by methods described elsewhere.[13] They were averaged over the conformational energy taken at intervals for 30° in φ and ψ, in the manner described above, for a temperature of 25°C. Contributions from conformations having energies more than 4 kcal mol^{-1} above the minimum energy were not included in the sums, in keeping with the procedure adopted for the evaluation of $\langle \mathbf{T}\rangle$ and, hence, of $\langle \mathbf{A}\rangle$.

In the limit $x_u \to \infty$ the diagonal components of the second moment tensor converge (relatively) to the same limit; i.e., $\langle x_\infty{}^2\rangle = \langle y_\infty{}^2\rangle = \langle z_\infty{}^2\rangle = x_u l_u{}^2 C_\infty/3$. The ratios $\langle x^2\rangle/\langle x_\infty{}^2\rangle$, etc., are plotted in Figure 3 against $1/x_u$. The components $\langle xy\rangle$, $\langle xz\rangle$, and $\langle yz\rangle$, not included in Figure 3, converge with chain length to their finite limits in a manner strikingly similar to the behavior of the first moments shown in Figure 2. Their limiting values, expressed as ratios to l_u^2, are 1.398, 11.58, and −1.288, respectively.

The second moment tensor formed from the displacement vector ρ (see eq 15 of the preceding paper) is similarly generated according to the relationship

$$\langle \rho^{\times 2}\rangle = \langle \mathbf{A}_{\rho[1}{}^{\times 2}\rangle \langle \mathbf{A}^{\times 2}\rangle^{x_u-2}\mathbf{A}_{x_u]}{}^{\times 2} \qquad (12)$$

where

$$\mathbf{A}_{\rho[1} = [\mathbf{T}, l_u - \mathbf{a}] \qquad (13)$$

and $\mathbf{A}_{x_u]}$ is defined by eq 10. Principal components $\langle \rho_1{}^2\rangle$, $\langle \rho_2{}^2\rangle$, and $\langle \rho_3{}^2\rangle$ of the diagonalized tensor are plotted against the reciprocal of the chain length in Figure 4, the moments being expressed as ratios to $x_u l_u{}^2$. Their convergence to the common intercept $C_\infty/3$ with increase in chain length is more gradual than for the first moments. Departures from the limit approximate 5% at $x_u = 165$, and ca. 2% at $x_u = 400$.

In Figure 5 the principal axes of $\langle \rho^{\times 2}\rangle$ are shown in three-point perspective relative to the first peptide unit and its axes X, Y, and Z. The gradations on the axes of both coordinate systems are in ångströms and also are shown in perspective. The positive direction of principal axis 1 lies beneath the XY plane and hence is not labeled. The plane defined by axes 1 and 3 has been omitted in order to avoid confusion in visualization of the systems in three dimensions.

Higher Moments

For the analysis of moments of higher rank we convert ρ to the reduced vector $\tilde{\rho}$ (see eq 19 of the preceding paper) employed in the investigations of PM and PDMS chains.[1,2] Thus, for the tensor of rank p we have

$$\langle \tilde{\rho}^{\times p}\rangle = \langle \tilde{\mathbf{A}}_{\rho[1}{}^{\times p}\rangle \langle \mathbf{A}^{\times p}\rangle^{x_u-2}\mathbf{a}_{x_u]}{}^{\times p} \qquad (14)$$

where

$$\tilde{\mathbf{A}}_{\rho[1} = \mathrm{diag}(\langle \rho_1{}^2\rangle^{-1/2}, \langle \rho_2{}^2\rangle^{-1/2}, \langle \rho_3{}^2\rangle^{-1/2})\mathbf{R}\mathbf{A}_{\rho[1} \qquad (15)$$

$\mathbf{R}$ being the matrix of the orthogonal transformation from XYZ to the normal coordinates. Averaging of the moment generator $\langle \mathbf{A}^{\times p}\rangle$ was performed as described above for a temperature of 25°C.

Six of the ten distinct elements of the reduced tensor of third rank $\langle \tilde{\rho}^{\times 3}\rangle$ are plotted against $1/x_u$ in Figure 6. Of the remaining four elements, $\langle \tilde{\rho}_1{}^2\tilde{\rho}_3\rangle$, $\langle \tilde{\rho}_1\tilde{\rho}_2\tilde{\rho}_3\rangle$, and $\langle \tilde{\rho}_2\tilde{\rho}_3{}^2\rangle$ are of smaller magnitude than $0.4\langle \tilde{\rho}_2{}^3\rangle$; $\langle \tilde{\rho}_1{}^2\tilde{\rho}_3\rangle$ lies between $\langle \tilde{\rho}_2{}^3\rangle$ and $\langle \tilde{\rho}_2{}^2\tilde{\rho}_3\rangle$ but is closer to the former. Both $\langle \tilde{\rho}_1\tilde{\rho}_2\tilde{\rho}_3\rangle$ and $\langle \tilde{\rho}_2\tilde{\rho}_3{}^2\rangle$ are positive for $x_u > 10$. Even–odd differences are apparent for chains with $x_u < 15$.

In Figure 7 the even components of the fourth moment tensor $\langle \tilde{\rho}^{\times 4}\rangle$ are plotted against $1/x_u$. The remaining tensor elements approach zero as x_u increases; they are small throughout the entire range shown. The linear portions of the curves in Figure 7 for the even moments exrapolate smoothly to their limiting values $\langle \tilde{\rho}_\kappa{}^2\tilde{\rho}_\lambda{}^2\rangle_0$. For $\kappa = \lambda$ (shown in Figure 7 as solid curves) this limit is 3 and for $\kappa \neq \lambda$ (shown as dashed curves) it is unity, as required for a spherically symmetric Gaussian distribution. With the exception of $\langle \tilde{\rho}_2{}^4\rangle$, all the even moments of the fourth moment tensor display a minimum in the region $1/x_u = 0.04$ to 0.05.

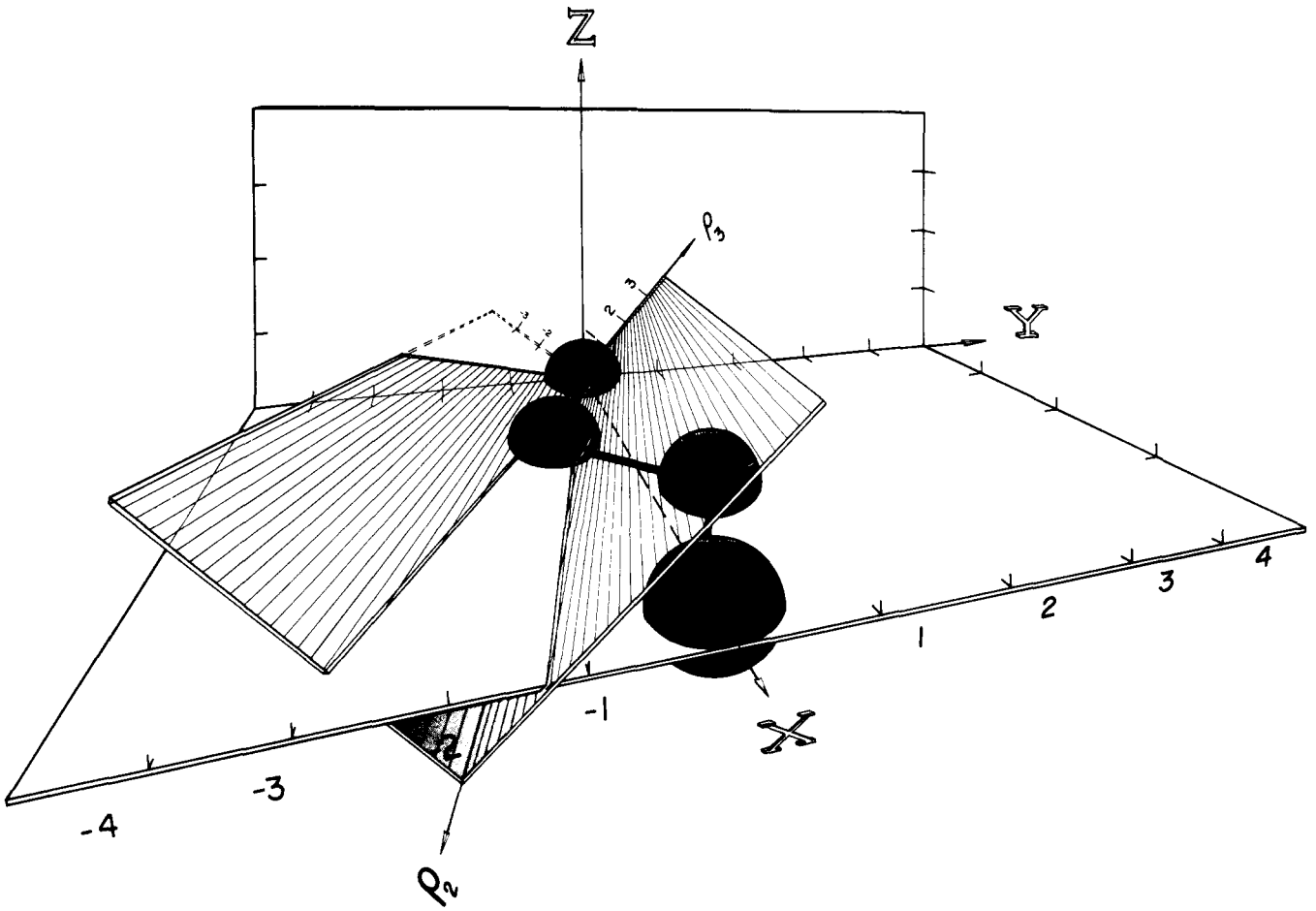

Figure 5. Principal axes of $\langle \rho^{\times 2} \rangle$ relative to the first peptide unit and its axes X, Y, and Z. The view of the figure is that of an observer located on a line from the origin to the vantage point having coordinates 5.7, −1.9, 4.4 in X, Y, Z.

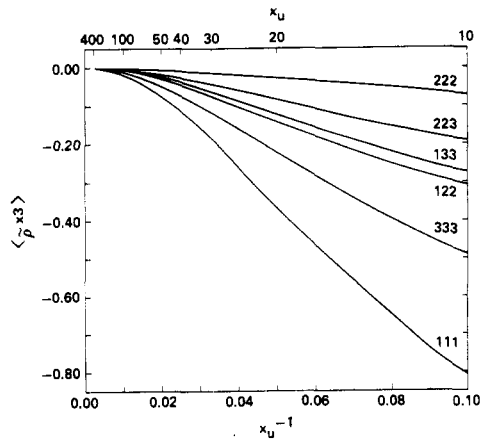

Figure 6. Components of the reduced third moment tensor $\langle \tilde{\rho}^{\times 3} \rangle$, with indices indicated by numerals, plotted against $1/x_u$.

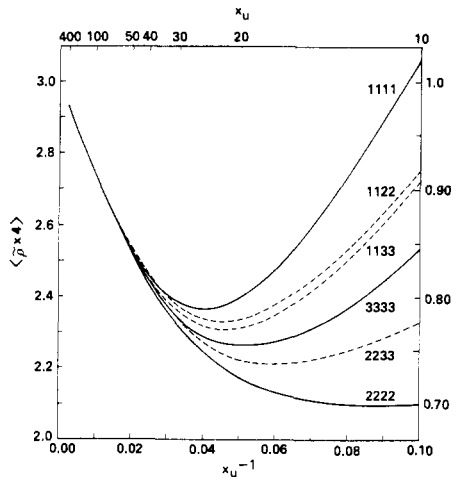

Figure 7. Even components of the reduced fourth moment tensor $\langle \tilde{\rho}^{\times 4} \rangle$ for PLA as a function of $1/x_u$. The principal components (left-hand ordinate scale) are plotted as solid lines and the mixed even components (right-hand ordinate scale) are indicated by dashed lines.

Convergences of the quantities $(\langle \tilde{\rho}_\kappa{}^{\times 2} \tilde{\rho}_\lambda{}^{\times 2} \rangle_0 - \langle \tilde{\rho}_\kappa{}^{\times 2} \tilde{\rho}_\lambda{}^{\times 2} \rangle)/\langle \tilde{\rho}_\kappa{}^{\times 2} \tilde{\rho}_\lambda{}^{\times 2} \rangle_0$ with increase in x_u for $x_u > 40$ are similar for the various even fourth moments. At $x_u = 100$, these quantities have values of ca. 0.083, and differences among them are less than 1% of this value. On the other hand, convergences of the odd reduced fourth moments (not included in Figure 7), as measured by departures from their Gaussian limits of zero, vary over a range of more than tenfold ($x_u \geq 40$). They are much smaller, however, than departures of the even fourth moments from their finite limits at the same chain length; hence, these variations are of minor significance.

The components of the fifth-rank tensor display a pattern similar to that of the third-rank tensors shown in Figure 6. The results in this respect resemble those for PDMS[1] and for PM (compare Figure 7 of ref 2). Skewness is greatest in the direction of axis 1, and least in the direction of axis 2. The predominant components of these tensors are

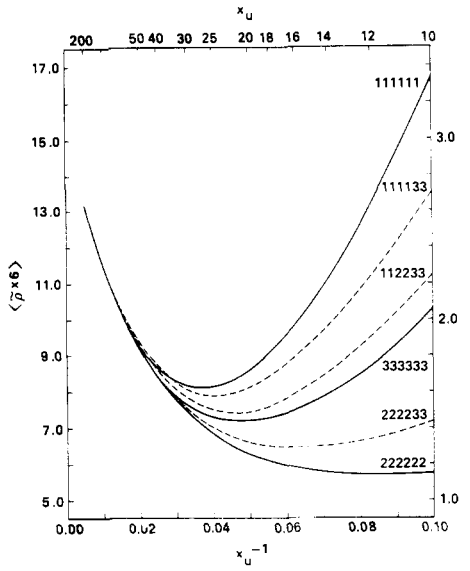

Figure 8. Even components of the reduced sixth moment tensor $\langle\tilde{p}^{\times 6}\rangle$ for PLA as a function of $1/x_u$. See legend for Figure 7. The component $\langle\tilde{p}_1^2\tilde{p}_2^2\tilde{p}_3^2\rangle$ has been multiplied by three.

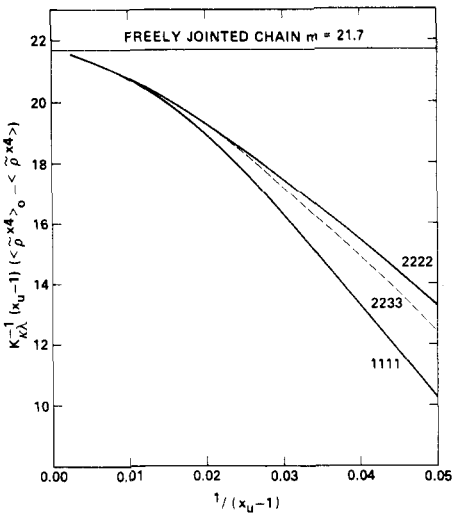

Figure 9. Differences between the elements of the reduced fourth moment tensor and their Gaussian limiting values, this difference being multiplied by $(x_u - 1)$ and divided by $K_{\kappa\lambda}$, then plotted against $1/(x_u - 1)$.

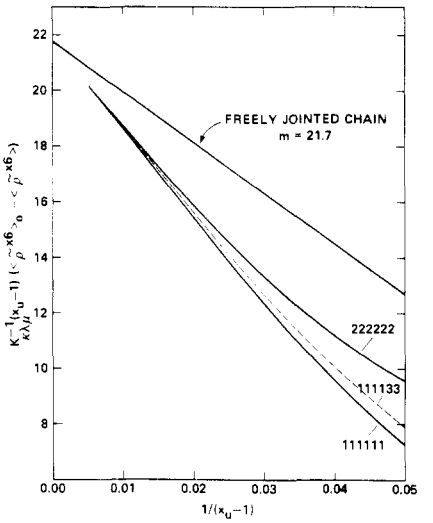

Figure 10. Differences between the elements of the reduced sixth moment tensor and their Gaussian limits treated as in Figure 9.

the homogeneous components $\langle\tilde{p}_1^5\rangle$ and $\langle\tilde{p}_3^5\rangle$ and those comprising an odd power of $\tilde{p}_1$ or $\tilde{p}_3$ in combination with an even power of $\tilde{p}_2$.

Six of the even components of the sixth moment tensor are shown as a function of $1/x_u$ in Figure 8. Their dependence on chain length resembles that of the analogous fourth moments shown in Figure 7; of the homogeneous elements $\langle\tilde{p}_1^6\rangle$ is greatest in magnitude and $\langle\tilde{p}_2^6\rangle$ is least. All the even components, with the exception of $\langle\tilde{p}_2^6\rangle$, display a minimum in the neighborhood of x_u = 20 to 25. For $x_u >$ 50, plots of the even sixth moments divided by their limiting values (15, 3, or 1, respectively) against $1/x_u$ are virtually coincident.

Comparing the rates of convergence of the moments of various ranks, we observe that, in general, the reduced third moments converge faster than the even fourth moments, but slower than the odd fourth moments. At x_u = 100, the deviations of the various components of the third moment tensor from the gaussian limit of zero range from 2.2×10^{-2} to 3.3×10^{-4}. Deviations in the neighborhood of 10^{-2}, which are of the same order of magnitude as those calculated for the even components of the fourth moment tensor (Figure 5), occur only for two of the homogeneous elements of the third moment tensor. Similarly, the fifth moments, in general, converge at rates intermediate between the convergences of the even and odd sixth moments; the convergences of the homogeneous fifth moments and the even sixth moments are similar.

Correlation with the Freely Jointed Chain

In Figure 9 the quantity $(\langle\tilde{p}^{\times 4}\rangle_0 - \langle\tilde{p}^{\times 4}\rangle)(x_u - 1)\, K_{\kappa\lambda}^{-1}$ is plotted against $1/(x_u - 1)$ for the indicated components of the fourth moment tensor (see eq 25 of the preceding paper). The three components shown are those possessing the largest, the smallest, and an intermediate value of the ordinant for given $x_u > 21$. Linearity is observed only for $x_u >$ 100. The relationship is approximately quadratic for $x_u >$ 50. Intercepts calculated from quadratic least-squares fitting of computed points for $x_u > 50$ yield m = 21.71 ± 0.06.

Deviations of the reduced even sixth moments from their Gaussian limits are treated correspondingly in Figure 10 (see the preceding paper). Three components showing the greatest, the least, and an intermediate divergence are shown. Intercepts calculated using quadratic least squares fits for $x_u > 50$ yield values of m for all of the even sixth moments that fall within the range 21.72 ± 0.02, in remarkable agreement with the value deduced from the fourth moments.

A corresponding analysis[14] of the fourth and sixth scalar moments $\langle r^4\rangle$ and $\langle r^6\rangle$ yields m = 21.5 ± 0.2. We conclude that correspondence with the freely jointed chain in the range of large x_u requires m = 21.7, this value being little dependent on the particular moments chosen for its evaluation.

The curves in Figures 9 and 10 exhibit large departures from the straight lines for the equivalent chain with m = 21.7 as the chain length decreases. The function plotted as ordinate magnifies the actual discrepancies betwen the equivalent chain and the real one. At $x_u - 1$ = 50 units (n^* = 50/21.7 = 2.30 equivalent bonds), the equivalent chain accounts for ca. 87 and 85% of the departures of the fourth and sixth reduced moments, respectively, from their asymptotic limits. At $x_u - 1$ = 100 units, these percentages are 95 and 94, respectively. We conclude that for $x_u > 50$ the real chain may be approximated fairly well by the free-

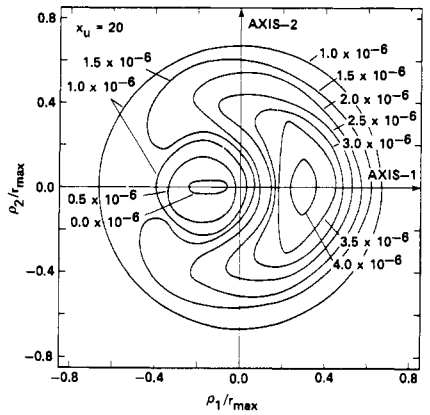

Figure 11. The density distribution function $W_a(\rho)$ of the displacement vector ρ in the plane of axes 1 and 2 for the PLA chain with $x_u = 20$. Contours of density given in Å^{-3} with each curve are obtained from $W_a(\rho)$ calculated according to eq 27 of the preceding paper truncated at $\nu = 6$.

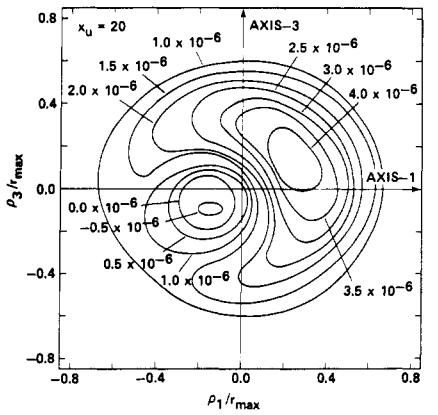

Figure 12. The density distribution $W_a(\rho)$ for $x_u = 20$ in the plane of axes 1 and 3. See legend to Figure 11.

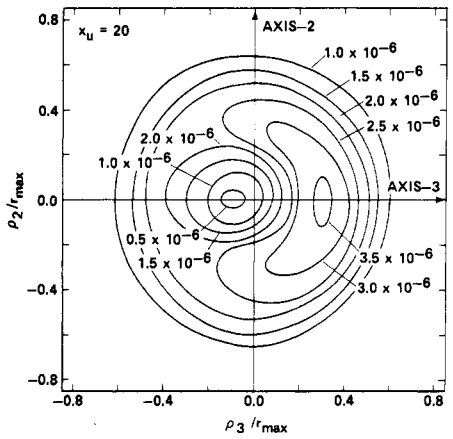

Figure 13. The density distribution $W_a(\rho)$ for $x_u = 20$ in the plane of axes 2 and 3. See legend to Figure 11.

ly jointed model. This correspondence is established in terms of the reduced displacement vector and its moments and not by direct comparison of moments of **r** (e.g., $\langle r^2 \rangle_0$), as in the modeling of the Kuhn equivalent chain.

It will be observed that if the value of m is taken to be a measure of chain extension, then PLA is appreciably more extended (or "stiffer") than PDMS with $m = 17.0$.[1] It is comparable to PM with $m = 20$. It is noted, however, that the analysis of the polypeptide chain is carried out in terms

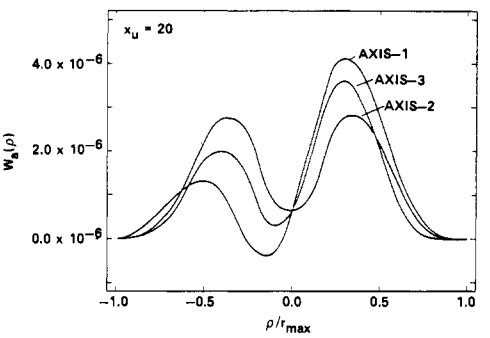

Figure 14. The density distribution function $W_a(\rho)$ of displacement vector ρ along axes 1, 2, and 3 for $x_u = 20$, in Å^{-3}. Densities calculated according to eq 27 of the preceding paper truncated at $\nu = 6$.

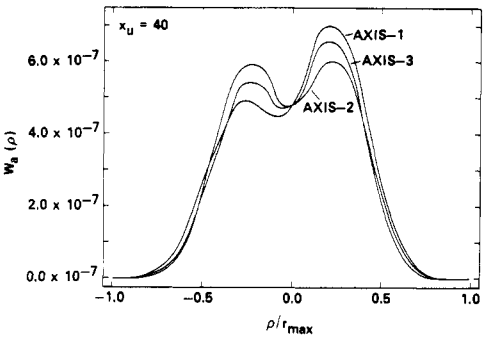

Figure 15. The density distribution $W_a(\rho)$ of displacement vector ρ along axes 1, 2, and 3 for $x_u = 40$, in Å^{-3}.

of virtual bonds. If actual bonds were employed, as for PDMS and PM, then the values of m required for PLA would be increased by a factor of 3 (the same reference frame XYZ being retained). On this basis, the PLA chain is much more extended than the other two.

Density Distributions

Density distributions $W_a(\rho)$ were calculated in the planes defined by the three pairs of principal axes using the three-dimensional Hermite expansion[9] (see eq 27 of the preceding paper) truncated at $\nu = 6$. Calculations were performed for PLA chains having 10, 20, 30, 40, 50, and 100 units. Only the results for $x_u = 20$ are included here. They are shown in Figures 11–13 in the form of contours of density expressed in Å^{-3} and plotted as functions of ρ/r_{max} where r_{max} denotes the length of the fully extended chain ($\varphi = 0°$ and $\psi = 0°$ for all residues; $r_{max} = 0.95\, x_u l_u$). Since the origin of the coordinates is displaced by **a** from $r = 0$, the maximum attainable value of ρ in any given direction generally differs from r_{max}.

The density contours shown in Figures 11, 12, and 13 for $x_u = 20$ reveal marked departures from spherical symmetry. With increase in x_u the distributions (not shown) become progressively less asymmetic. Those for $x_u = 100$ consist of nearly concentric circles, indicating approach to spherical symmetry.

Axes of symmetry are evident in Figures 11, 12, and 13 located along axis 1, at an angle of approximately 30° from axis 1, and along axis 3. These features are peculiar to the planes shown; they do not apply to the distributions in three dimensions, for which neither axes nor planes of symmetry are evident.

Densities along each of the three principal axes are plotted against ρ/r_{max} for $x_u = 20$ and $x_u = 40$ in Figures 14 and 15, respectively. For $x_u = 20$, absolute maxima occur along

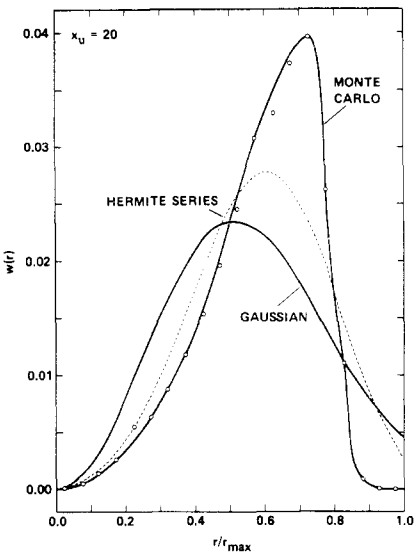

Figure 16. Radial distributions $w(r)$ in Å^{-1} for PLA with $x_u = 20$. The dashed curve has been obtained by numerical integration over $W_a(\rho)$ from the three-dimensional Hermite series truncated at $\nu = 6$. Points and the associated curve represent results for Monte Carlo configurations generated using the expectation values for φ, ψ conformations at 30° intervals. The Gaussian curve represents the spherically symmetric Gaussian calculated from $\langle r^2 \rangle$ for $x_u = 20$.

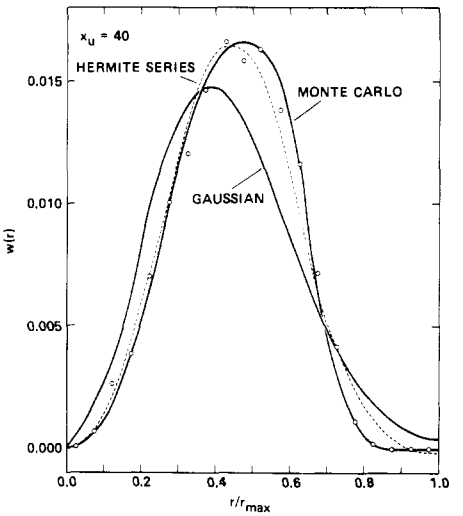

Figure 17. Radial distributions calculated for PLA with $x_u = 40$. See legend for Figure 16.

each of the axes at $\rho/r_{max} = 0.30 - 0.35$. Minima occur between −0.15 and 0, and secondary maxima from −0.50 to −0.35. The density distribution along axis 2 is nearly symmetric about $\rho_2/r_{max} = 0$.

The calculated densities are negative along axis 1 over the range $-0.25 < \rho_1/r_{max} < -0.05$. This is of course indicative of the inadequacy, for short chains, of the Hermite series truncated at $\nu = 6$.[1,2] Negative calculated densities vanish for $x_u > 30$.

When $x_u = 40$ (Figure 15), the densities $W_a(\rho)$ along the three principal axes display absolute maxima near $\rho/r_{max} = 0.20$, secondary maxima at ca. −0.25 and minima near 0. The distribution along axis 2 remains symmetrical about $\rho_2/r_{max} = 0$ while those about axes 1 and 3 display less asymmetry than for $x_u = 20$. At $x_u = 50$ (not shown) densities along each of the axes are approximately symmetric about $\rho = 0$. Shallow minima occur near $\rho_i/r_{max} \simeq 0$ along each axis. At $x_u = 100$, the distribution is approximately spherical about $\rho = 0$, i.e., about $\mathbf{r} = \mathbf{a}$.

Radial Distributions

Radial distribution functions evaluated by numerical integrations (performed using Simpson's rule) over the Hermite densities $W_a(\rho)$ calculated above are shown by dashed curves in Figures 16 and 17 for chains of $x_u = 20$ and 40 units, respectively. Included also for comparison are the curves for the spherical Gaussians centered at $\mathbf{r} = 0$ for chains of the same length. Marked departures from Gaussian behavior are apparent.

For the Monte Carlo calculations, the 44 pairs of angles φ, ψ at 30° intervals for which the computed conformational energy does not exceed 4 kcal mol^{-1} were assigned expectations given by the Boltzmann factors of their energies. Conformations were generated from sets of random numbers with intervals for each state chosen to match its expectation value. A total of 2500 chains of 100 bonds were generated in this manner and the magnitude r of the end-to-end vector for each was computed. Since the conformations of adjacent residues in the polypeptide chain are independent, it is legitimate to evaluate r for shorter sequences of 10, 20, . . . , 50 units from within the 100-bond chains. Absence of correlations between the chain sequences thus sampled is assured by the independence of the conformations of neighboring units. Computer time was thus conserved.

The results of the Monte Carlo calculations, plotted for convenience at intervals of $r_{max}/20$, are shown as circles in Figures 16 and 17 for $x_u = 20$ and 40, respectively. The solid curves approximate the individual points. The density distributions calculated by means of the Hermite series expansion and the Monte Carlo methods differ significantly, for $x_u = 20$. At $x_u = 40$, however, the two distributions are in good agreement. Departures from Gaussian remain significant, however, at $x_u = 40$.

Acknowledgment. The authors acknowledge with gratitude the assistance of Dr. Michael Conrad who kindly prepared Figure 5 in perspective. This work was supported by the National Science Foundation, Grant No. DMR-73-07655 A01.

References and Notes

(1) P. J. Flory and V. W. C. Chang, *Macromolecules*, preceding paper in this issue.
(2) D. Y. Yoon and P. J. Flory, *J. Chem. Phys.*, **61**, 5366 (1974).
(3) D. A. Brant and P. J. Flory, *J. Am. Chem. Soc.*, **87**, 2791 (1965).
(4) G. N. Ramachandran, C. Ramakrishnan, and V. Sasisekharan, *J. Mol. Biol.*, **7**, 95 (1963).
(5) D. A. Brant, W. G. Miller, and P. J. Flory, *J. Mol. Biol.*, **23**, 47 (1967).
(6) S. Premilat and J. Hermans, *J. Chem. Phys.*, **59**, 2602 (1973).
(7) F. Th. Hesselink, *Biophys. Chem.*, **2**, 76 (1974).
(8) P. J. Flory, *Proc. Natl. Acad. Sci. U.S.A.*, **70**, 1819 (1973); *Macromolecules*, **7**, 381 (1974).
(9) P. J. Flory and D. Y. Yoon, *J. Chem. Phys.*, **61**, 5358 (1974).
(10) D. A. Brant and P. J. Flory, *J. Am. Chem. Soc.*, **87**, 2788 (1965).
(11) S. Tanaka and A. Nakajima, *Polym. J.*, **2**, 717 (1971).
(12) P. Doty, J. H. Bradbury, and A. M. Holtzer, *J. Am. Chem. Soc.*, **78**, 947 (1956).
(13) P. J. Flory and Y. Abe, *J. Chem. Phys.*, **54**, 1351 (1971).
(14) R. L. Jernigan and P. J. Flory, *J. Chem. Phys.*, **50**, 4165 (1969).
(15) Premilat and Hermans[6] calculate **a** in a reference frame *preceding* the one belonging to the first unit counted in summing contributions of the virtual bond vectors l_u for units 1 to x_u. Thus, their persistence vector $\mathbf{a}_{PH}$ is related to ours according to $\mathbf{a}_{PH} = \langle \mathbf{T} \rangle \mathbf{a}$. For the infinite chain, therefore, $\mathbf{a}_{PH} = \mathbf{a} - l_u$.